

# Creating New VLS Silicon Nanowire Contact Geometries by Controlling Catalyst Migration

Sardar B. Alam,<sup>†</sup> Federico Panciera,<sup>‡,§</sup> Ole Hansen,<sup>†,||</sup> Kristian Mølhave,<sup>\*,†</sup> and Frances M. Ross<sup>\*,§</sup>

<sup>†</sup>Department of Micro- and Nanotechnology, Technical University of Denmark, DK-2800 Kgs. Lyngby, Denmark

<sup>‡</sup>Department of Engineering, University of Cambridge, Cambridge CB2 1TN, United Kingdom

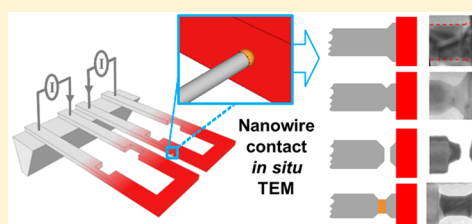
<sup>§</sup>IBM T.J. Watson Research Center, Yorktown Heights, New York 10598, United States

<sup>||</sup>Center for Individual Nanoparticle Functionality, Technical University of Denmark, DK-2800 Kgs. Lyngby, Denmark

## Supporting Information

**ABSTRACT:** The formation of self-assembled contacts between vapor–liquid–solid grown silicon nanowires and flat silicon surfaces was imaged in situ using electron microscopy. By measuring the structural evolution of the contact formation process, we demonstrate how different contact geometries are created by adjusting the balance between silicon deposition and Au migration. We show that electromigration provides an efficient way of controlling the contact. The results point to novel device geometries achieved by direct nanowire growth on devices.

**KEYWORDS:** Nanowire integration, Si nanowire growth, CVD, in situ manipulation, TEM, cantilever



The vapor–liquid–solid (VLS) mechanism,<sup>1</sup> a metal-catalyzed chemical vapor deposition (CVD) process, is a prominent and versatile bottom-up technique for fabricating silicon nanowires, enabling the creation of large arrays of nanowires with controlled structure. Nanowires grown by the VLS mechanism have a wide range of possible applications: in electronics,<sup>2</sup> solar cells,<sup>3</sup> batteries,<sup>4</sup> optoelectronic devices including light-emitting diodes,<sup>5</sup> lasers,<sup>6</sup> and photodetectors,<sup>7</sup> thermoelectric devices,<sup>8</sup> electromechanical devices like resonators<sup>9</sup> and piezoelectric generators,<sup>10</sup> as well as biological<sup>11</sup> and chemical sensors.<sup>12</sup> The performance of silicon nanowire-based devices depends not only on the nanowire characteristics but also the way in which the nanowires interface with the rest of the circuit, that is, the intricate details of the electrical connections between each nanowire and the larger scale device.

Recent studies<sup>13–15</sup> have opened the possibility of creating VLS Si nanowire-based devices where the nanowire grows toward and touches an opposing surface to form a self-assembled contact. This mechanical and electrical connection is formed catalytically by the metal–Si eutectic droplet at the tip of the wire and can result in an epitaxial Si–Si junction.<sup>14</sup> Recently, such self-assembled contacts have enabled one-step integration of VLS nanowires into transistors,<sup>16</sup> mechanical resonators<sup>17,18</sup> and sensors<sup>19</sup> by direct growth on devices heated in a CVD reactor. Nanowire growth can also be achieved at locally heated regions of a microchip system in a gas environment.<sup>20,21</sup> The direct integration of VLS nanowires in device architectures circumvents the integration issues that arise with transferring VLS grown nanowires from a substrate to the device.<sup>22,23</sup> But for direct integration of nanowires in practical applications using self-assembled contact formation, as well as for developing new types of devices, it is important to

understand the process that creates the contacts and define techniques to control the contact geometry.

Here we present real time observations, made in situ in a transmission electron microscope (TEM), of the physical processes that occur during the formation of self-assembled nanowire contacts. In situ TEM not only allows real time observation of the contact formation process but also enables tracking the outcome of varying different parameters with the aim of controlling the type of contact created. We demonstrate that the geometry of the contact between a nanowire and a large scale structure (i.e., a flat surface) can be controlled by varying the contact surface temperature and the current through the nanowire during contact creation. These parameters control the Si growth rate and the migration and diffusion of the liquid catalyst at the instant when the nanowire contacts the surface. We show that the balance of growth versus migration and diffusion gives rise to a variety of contact geometries relevant to electronic and nanomechanical devices.

To form contacts in situ, silicon nanowires were grown on silicon cantilever heaters to bridge from one cantilever to an adjacent cantilever.<sup>20</sup> The cantilevers, fabricated on silicon-on-insulator chips, have {111} sidewalls on which nanowires grow perpendicularly in the <111> direction. Adjacent cantilevers are separated by gaps of 2–3  $\mu\text{m}$  (see [Supporting Information](#)). Chips containing cantilever arrays were cleaned with HF vapor, transferred to the ultrahigh vacuum (UHV) system, and 2–5 nm Au was evaporated before vacuum transfer to the UHV-TEM, a Hitachi H-9000.<sup>24</sup> Pairs of adjacent cantilevers were

Received: June 2, 2015

Revised: August 24, 2015

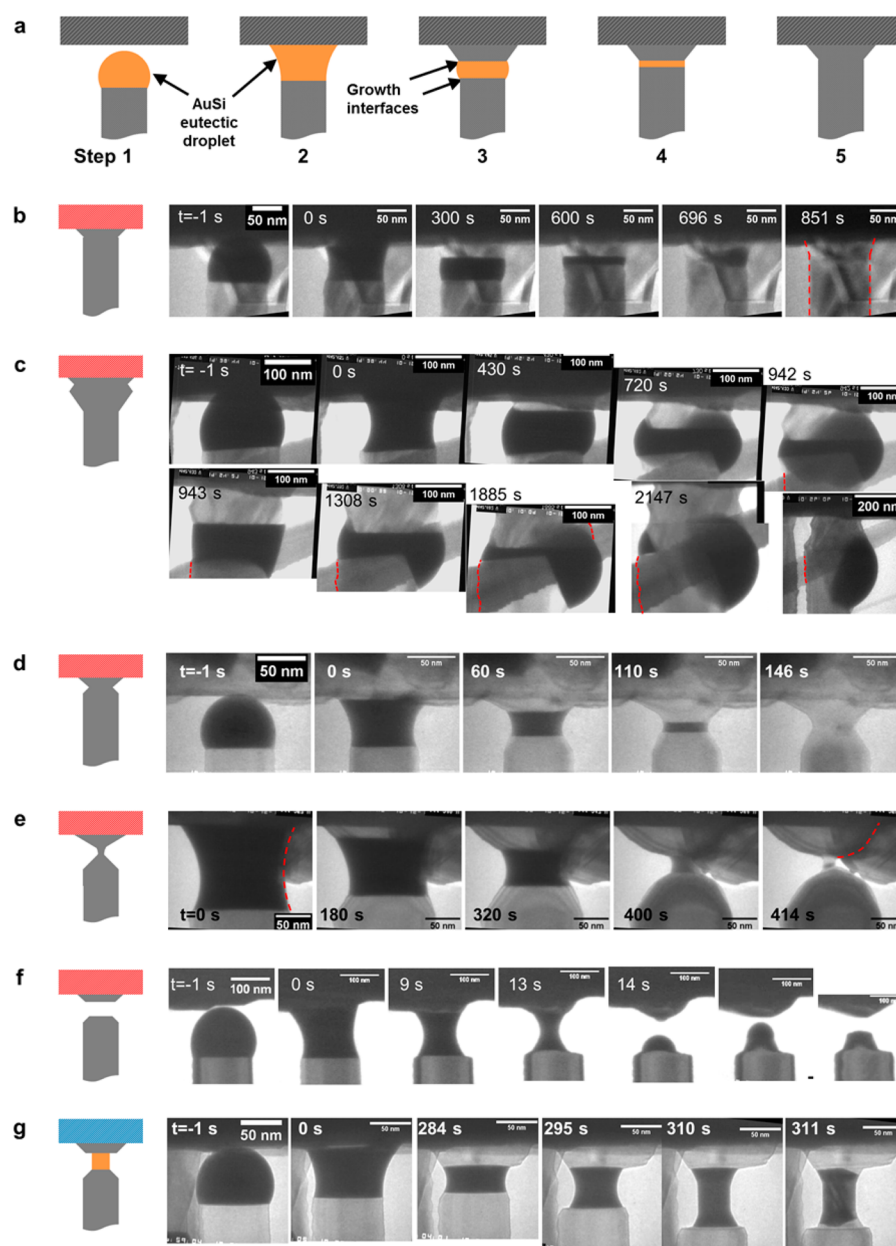


**Figure 1.** (a) Schematic steps in contact formation: (1)  $t < 0$  s, free nanowire approaches the receiving cantilever, (2)  $t = 0$  s, moment of contact, when the AuSi catalyst wets the receiving cantilever, (3–4)  $t > 0$  s, Au migrates from contact site while Si is being deposited, and (5) process completion, when final Si–Si contact is created. (b–h) Examples of each observed type of contact geometry. (b) Straight contact, created when Si deposition rate  $\approx$  AuSi eutectic shrinkage rate. The angled contrast is due to a separate, out-of-focus nanowire that overlaps the nanowire of interest. (c) Bulged Si–Si contact with Si deposition rate  $>$  AuSi eutectic shrinkage rate. The final frame shows a lower-magnification image to clarify the geometry, including an angled nanowire that crosses in projection, but is some distance from the nanowire making contact. (d) Necked Si–Si contact with Si deposition rate  $\lesssim$  AuSi eutectic shrinkage rate. (e) Extremely necked Si–Si contact with Si deposition rate  $<$  AuSi eutectic shrinkage rate. (f) Gap, where Si deposition rate  $\ll$  AuSi eutectic shrinkage rate. (g) Si–Au–Si contact created by cooling the system during contact formation; in this nanowire, the eutectic is stretched from 35 to 65 nm as the cantilevers contract on cooling at 310 s. The red lines in (b,c,e) indicate the growing nanowire of interest, to distinguish from overlapping, out of focus nanowires.

heated by two independent power sourcemeters operating in constant current mode. On heating to temperatures in the range 470–530 °C and flowing disilane ( $\text{Si}_2\text{H}_6$ ) at pressures of  $1\text{--}20 \times 10^{-6}$  Torr, the Au agglomerated and formed AuSi droplets that catalyzed nanowire growth, yielding diameters in the range 40–160 nm. Self-assembled contact formation is initiated when a nanowire grown from one cantilever (referred to as the “origin cantilever”), impinges on the opposing flat sidewall of the adjacent cantilever (the “receiving cantilever”), Supporting Information Figure S1. During or after contact

formation, current could be passed through the bridging nanowire by using a third sourcemeter connected between the cantilevers; this sourcemeter could also measure any current that flowed on contact due to small voltage differences between the cantilevers.

Schematics of the observed contact formation process and the different geometries created by adjusting the conditions are shown in Figure 1. By controlling the pressure, the temperatures of each cantilever, and the current through the nanowire, we created Si–Si contacts with straight (Figure 1b), bulged

(Figure 1c), and necked profiles (Figure 1d and 1e), as defined by comparing the width at the contact to the nanowire diameter. Particular choices of conditions also formed nanogaps (Figure 1f) and Si–Au–Si contacts (Figure 1g).

The contact formation process, illustrated in the schematic in Figure 1a for a straight contact and shown in Movie 1 for a straight and Movie 2 for a necked contact, proceeds as follows: when the impinging wire (step 1) makes contact with the receiving cantilever at  $t = 0$  s (step 2), the AuSi eutectic droplet wets the sidewall of the destination cantilever and its geometry is transformed to a hyperboloid sandwiched between the nanowire and sidewall. This sandwiched droplet catalyzes further epitaxial growth (step 3–4) until a Si–Si contact is created (step 5). There are two liquid–solid interfaces from which epitaxial growth could proceed: one growth front is at the AuSi eutectic/nanowire interface, while the second growth front is at the eutectic/cantilever interface (step 2–4). Meanwhile, several processes (coarsening, electromigration) may drive Au away from the contact site, as discussed below. The process is completed when either the two Si interfaces meet or Au migration breaks the connection and a gap forms.

The observations in Figure 1 indicate that the contact morphology is determined by the competition between the rate of migration of Au away from the contact site and the rate of Si deposition. To create a Si–Si contact, sufficient AuSi eutectic should remain at the contact site to ensure catalyzed Si growth proceeds. If the Au migration rate is higher than the Si deposition rate, the two growth interfaces reduce in area as the eutectic volume decreases and a necked contact forms. If Au migration is even faster, Au diffuses away before the Si grows far enough to make contact and a nanogap is created. On the other hand, if the Au migration rate is much lower than the Si deposition rate, a bulged contact is created where the contact is wider than the nanowire. In the bulged case, the growth interfaces increase in area as the liquid is squeezed between the two progressing Si growth fronts. When Au migration and Si deposition rates are comparable, straight contacts are created with the diameter of the contact structure almost the same as the wire. There is still some widening of the contact at its interface to the cantilever, as the wetting angle of the liquid eutectic increases as contact formation proceeds. The resulting morphology is similar to the early stages of nanowire growth, where the base of a nanowire is wider than its eventual diameter.<sup>25</sup>

If the contact formation process is interrupted by cooling, a sandwiched Si–Au–Si contact can be created. The contact in Figure 1g was created when the contact formation process was interrupted by simultaneously shutting off the heating current to the two cantilevers. Si–Au–Si contacts can also be created when the receiving cantilever is cold, as previously demonstrated.<sup>15</sup>

In order to control the contact morphology, we need to understand and control the factors determining the rates of Si growth and Au migration. Under the conditions used here, the Si growth rate in a freestanding nanowire is well-known to be proportional to pressure, independent of diameter, and have an Arrhenius dependence on temperature.<sup>26</sup> During the contact process, a complex geometry with two growth fronts is present, but we find that the growth rate overall actually follows fairly simple kinetics. When the droplet first touches the cantilever, Si continues to deposit. Its growth rate is similar to the precontact rate for contacts that end up straight or bulged. In necked contact cases, higher growth rates (by up to 2 $\times$ ) can be seen, as

discussed below. Growth then proceeds from either interface, but only one at a time (Figures 1d and 2a). In other words, we generally observe that growth halts on one interface during deposition on the other. In the overall data set, we found no clear correlation with temperature, interface diameter, wetting angles, or bias voltage across the wire that could predict which

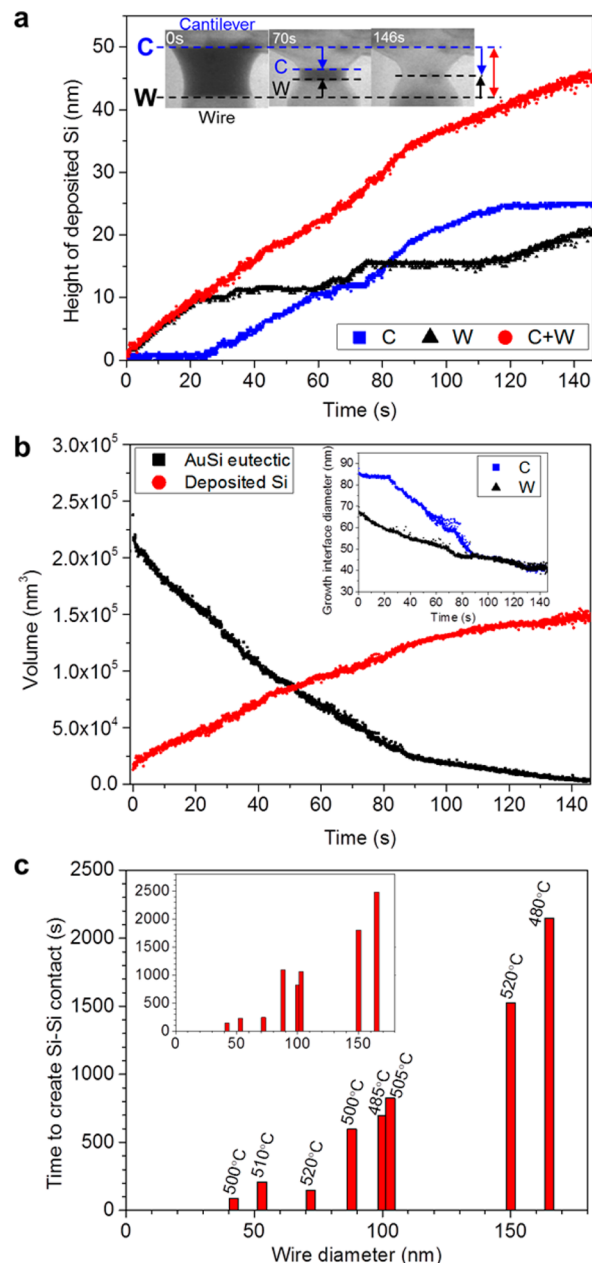


**Figure 2.** (a) Thickness of the Si deposited at the cantilever and nanowire side (C and W) for the necked contact case depicted in Figure 1d, and the total thickness of Si deposited showing an approximately constant rate. (b) Volume of AuSi eutectic and volume of deposited Si for the same contact. The inset shows the diameters at the two AuSi–Si interfaces decreasing in width, creating a necked contact. (c) Time to complete Si–Si contact plotted against nanowire diameter. The contact is said to be complete when the two growth fronts meet. Because the data were obtained at different pressure and temperature, the inset shows the same plot but with times scaled to conditions of  $1 \times 10^{-5}$  Torr disilane and 500 °C, using the linear dependence on pressure and Arrhenius dependence on temperature.<sup>26</sup>

interface would be growing. Si deposition from the super-saturated eutectic initiates at the lowest-energy site for ledge nucleation.<sup>24</sup> We suggest that this location may switch from one interface to the other depending on subtle details of liquid geometry or surface structure on different parts of the nanowire, which change as the geometry develops during contact formation. Adding the two growth curves, one from each interface, gives an approximately constant rate of deposited Si (Figure 2a). The rate eventually decreases with time as the collection area of the catalyst (AuSi surface area) decreases during the contact process. However, the Si growth rate does not depend only on the liquid surface area. In addition to Si collected from the gas phase at the AuSi surface, there is an additional source of Si, the atoms originally in the AuSi eutectic. These are precipitated as the eutectic volume shrinks due to Au migration. This effect is analogous to the enhanced growth seen in nanowires that are tapering due to a shrinking catalyst droplet<sup>26</sup> and are also the reason necked contacts have higher growth rate than prior to contact. At the growth temperatures used here, the Si content of the eutectic is around 23–25% on the Si rich side of the phase diagram.<sup>27</sup> Although the Si in the eutectic is not enough to bridge the hyperbolic geometry made upon the initial wetting, the migration of Au should therefore provide a noticeable additional contribution to the growth rate to achieve solid Si contacts. Figure 2b shows the evolution of the AuSi volume with time for the contact process shown in Figures 1d and 2a. In the early stages of the contact formation process ( $t < 60$  s), the eutectic volume decreased at a rate of  $2400 \text{ nm}^3/\text{s}$ ; the total Si deposition rate was  $1300 \text{ nm}^3/\text{s}$  of which  $\sim 570 \text{ nm}^3/\text{s}$  is from Si segregation from the eutectic.

Given the approximately constant Si growth rate, one would expect the total time to complete the Si–Si contact (when the two growth fronts meet) to be approximately proportional to wire diameter. This is simply because when a larger wire touches the opposing cantilever at  $t = 0$  s, the growth interface is proportionally further from the cantilever surface because the droplet is proportionally larger. Figure 2c confirms an approximately linear relationship, once the measured times to contact are corrected for the pressure and temperature of each experiment.<sup>26</sup>

It is now clear how the geometry of the contact depends on the balance of Au migration rate and Si deposition rate. For example, the formation of a nanogap depends on whether the Au migration rate is fast enough to move all the AuSi liquid from the contact region before the time, given approximately in Figure 2c, that would have been required to complete the contact between the interfaces. Also, the necked morphology of the contact in Figure 2a, b is a consequence of shrinking of the growth interface diameters as the eutectic volume decreases at a higher rate than silicon deposition. Bulged contacts are expected when Au migration is slow, giving more time to incorporate Si from the gas phase.

These qualitative conclusions are quantified in Figure 3a where we show the relationship between Au migration (the rate of change of AuSi volume measured at the start of the contact process), Si deposition (the volumetric deposition rate, also measured at the start of the contact process), and morphology (ratio of diameter at the middle of the final contact to initial nanowire diameter). The geometry of the self-assembled contact correlates with the ratio. Nanogaps form above the 1:1 line, necked and straight contacts at the line, and bulged contacts below the line. Although, according to the discussion

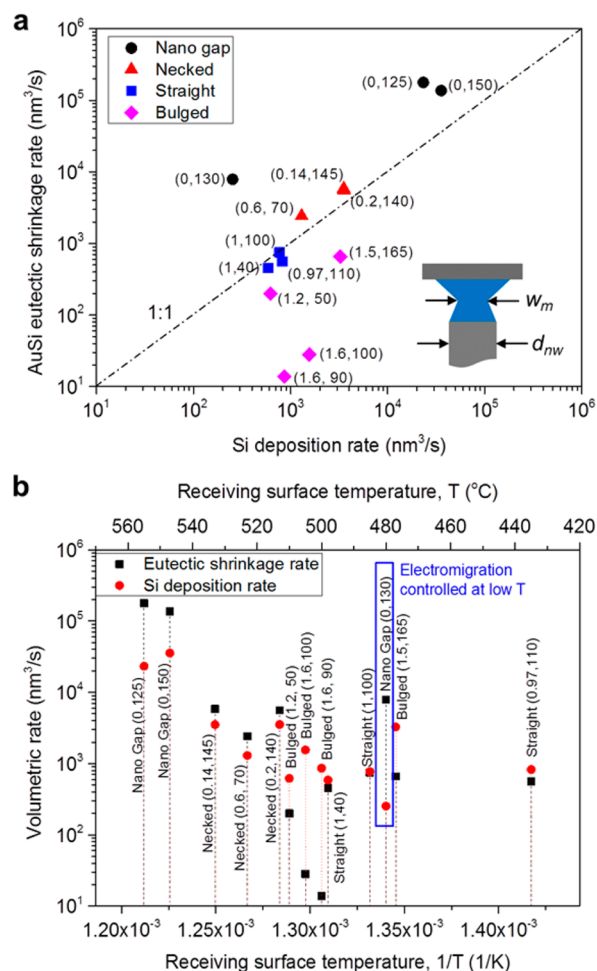


**Figure 3.** (a) Eutectic shrinkage rate and Si deposition rate shown for different nanowires with a 1:1 guiding line. These values are calculated at the initial time of contact. The geometry of the eventual contact is shown by color and shape. The initial conditions appear to correlate with the final structure. The numbers next to each data point provide a quantitative measure of the contact geometry. The first is the ratio of contact width  $w_m$  to wire diameter  $d_{nw}$ , so that large numbers represent bulged contacts, small ones necked, and zero represents a nanogap. The second number is the wire diameter  $d_{nw}$  in nm. (b) The same data plotted against inverse temperature. The comparison of the two rates (whether the black dot is above or below the red) correlates with morphology, as expected from (a). The electromigration experiment marked with blue is discussed in the text. A pressure corrected version of (b) can be found in the Supporting Information.

above, nanowire diameter should play a role in determining the morphology, it appears not to be a controlling factor. This is presumably because the range of variation in diameter is only a factor of 4 in these experiments, while the Si deposition and Au migration rates span a much larger range. The Si deposition rate spans 2 orders of magnitude and is overall consistent with the expected Arrhenius dependence (Figure 3b). The migration rate spans 4 orders of magnitude and is not well correlated with temperature at the contact site; it will be discussed in more detail below. Clearly a highly enhanced Au migration process is involved in the necked and gap contact cases.

The data in Figure 3 provides insights into which parameters to control in order to create a particular contact geometry for a given nanowire. We first consider the Si deposition rate. This can be increased by raising the temperature, but this is perhaps

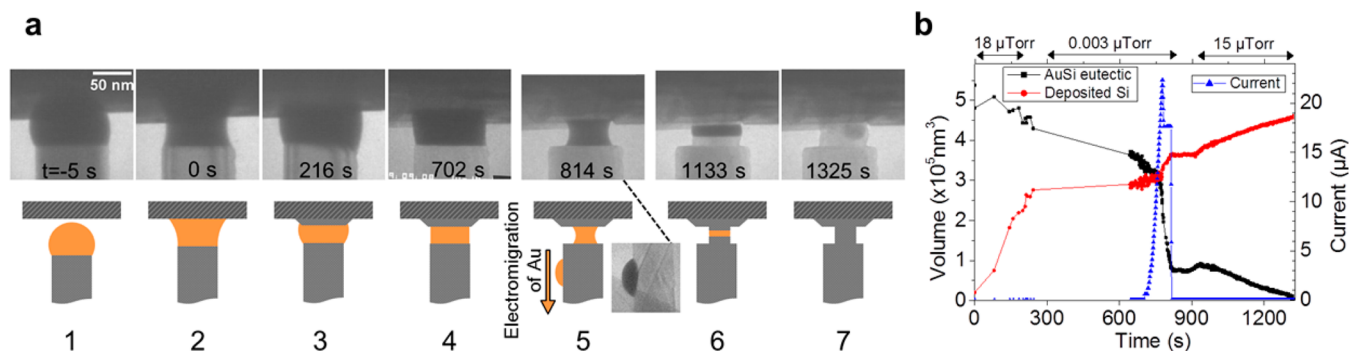


**Figure 4.** Controlled contact diameter created through pressure and electromigration: (a) Structure and schematic, and (b) volumetric and nanowire current data. (a1) Before contact. (a2)  $t = 0$  s, initial contact and early stage of contact formation with the eutectic shrinking at  $290 \text{ nm}^3/\text{s}$  and Si deposition at  $1130 \text{ nm}^3/\text{s}$ . Nanowire and contact site are at  $475 \pm 10 \text{ }^\circ\text{C}$ , pressure  $18 \text{ } \mu\text{Torr}$ . (a3) Bulged contact starting to form. The disilane was then reduced to  $10^{-9} \text{ Torr}$ . (a4) Contact evolves toward a necked geometry with the eutectic shrinking at  $200 \text{ nm}^3/\text{s}$  and Si growth rate slow (and impractical),  $\sim 50 \text{ nm}^3/\text{s}$ . (a5) Voltage applied across nanowire. At  $3 \text{ V}$  ( $27 \text{ } \mu\text{A}$ , current density  $3700 \text{ } \mu\text{A}/\mu\text{m}^2$ ), eutectic shrinkage was rapid,  $4900 \text{ nm}^3/\text{s}$ , with  $1200 \text{ nm}^3/\text{s}$  Si deposition from segregation. This voltage pulse removes a volume of AuSi that would have taken 16 min in the absence of electromigration. The Au was observed moving in the direction of the electron current along the nanowire toward the origin cantilever (inset image). (a6) Voltage back to  $0 \text{ V}$ , disilane pressure restored at  $\sim 15 \text{ } \mu\text{Torr}$ ; a narrowed Si–Si contact formed. During this phase the eutectic shrinkage and Si deposition rate were similar, about  $200 \text{ nm}^3/\text{s}$ , leading to a straight contact with  $60 \text{ nm}$  diameter. (a7) Final contact geometry.

not a straightforward approach because temperature will also affect Au migration, making it hard to predict the result. Changing the pressure is a better strategy, as pressure has little direct effect on Au migration rate.<sup>28</sup> Figure 4(a1–a4) shows a case where pressure was reduced to allow time for Au to migrate, initiating a necked structure under conditions that were previously forming a bulged contact. However, the range of pressures that can be applied yet still obtain reasonable Si growth rates is relatively limited. Instead, migration of Au appears to be the best parameter to control, because as shown in Figure 3 it can evidently display a large range of values in different experiments. But what drives the Au migration? Several different mechanisms are possible: Ostwald ripening, diffusion driven by a surface coverage concentration gradient, thermomigration, and electromigration. We discuss these mechanisms in the Supporting Information and conclude that for the conditions of the experiments, electromigration is the dominant mechanism. Electromigration can explain the observation in Figure 3b of the very different migration rates seen in otherwise similar experiments: small voltage differences (see Supporting Information) between the origin and receiving cantilever, arising from slight differences in cantilever resistance even when the heating currents are the same, can drive an  $\sim 1 \text{ } \mu\text{A}$  current through the nanowire at the moment of contact, forcing Au motion.

The dominance of electromigration allows us to control the contact structure in a practical way. We install a sourcemeter between the adjacent cantilever legs (see Supporting Information Figures S1 and S2b) to control the current through the bridging nanowire after the moment of first contact. In Figure 3b, a current flow of  $11 \text{ } \mu\text{A}$  after initial contact led to a nanogap in the low temperature of the plot where the migration rate is otherwise low. In Figure 4(a5),b, a pulse of current, several minutes after contact, moved Au and reduced the contact area from  $100$  to  $60 \text{ nm}$  diameter. The current pulse gives a clear corresponding reduction in eutectic volume and increase in Si by segregation. It is interesting to note that control via electromigration in principle does not require direct observation in a TEM as currents through the wire are indicators of contact process initiation. It is clear from this example that the use of current flow to drive electro-

migration is a versatile approach to creating complex contact geometries.

Having developed a protocol for creating different types of contacts, we can probe the electrical properties of the resulting nanowire bridges in situ (Figure 5). Because each microcanti-

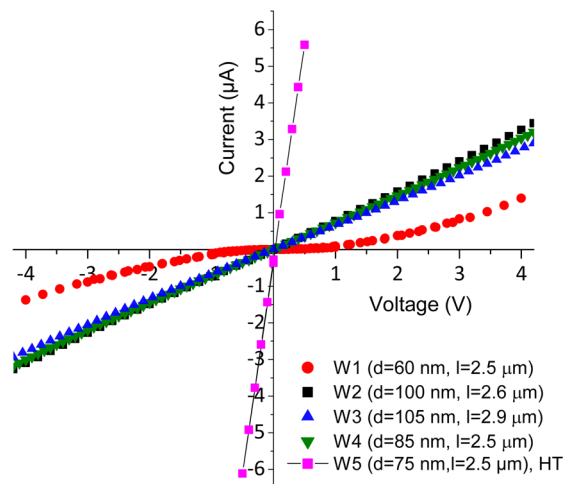


**Figure 5.**  $I$ – $V$  characteristics measured for four bridging nanowires (W1 to W4) for a voltage range of  $-4$  to  $4 \text{ V}$ . Measurements made at RT in situ on silicon dioxide-free nanowires with  $\sim 1/3$  monolayer of Au on the surface.<sup>30</sup> W2 and W4 are the nanowires in Figure 1b with Si–Si contact and Figure 1g with Si–Au–Si contact, respectively. Wire diameter ( $d$ ) and length ( $l$ ) are given in the legends. (W5) Another nanowire measured at a high temperature (HT) of  $480 \text{ }^\circ\text{C}$ .

lever heater has two contacts leads, in situ four-point measurements on oxide-free bridging nanowires are possible. At room temperature (RT), the bridges typically exhibit linear Ohmic  $I$ – $V$  characteristics at bias voltages up to about  $4 \text{ V}$ . Thinner wires show higher resistance, as seen by comparing wires W1 and W2. The resistivities are of the order  $0.3$ – $1.5 \text{ } \Omega\text{cm}$ , consistent with previous measurements.<sup>15,29</sup> At the growth temperature, the higher carrier density leads to higher current densities than at RT, as illustrated in Figure 5.

To summarize, in situ observations show the formation of contacts between Au catalyzed silicon nanowires and a flat Si surface and demonstrate that the final geometry of the contact structure is governed by the relationship between the Si deposition rate and the rate at which the eutectic volume shrinks with time. By controlling the pressure, temperature, and current through the nanowire, we can control the balance between Si growth and the eutectic shrinkage due to Au diffusion and electromigration to create contact structures of desired geometries including straight, necked, and bulged Si–Si contacts, nanogaps, and Si–Au–Si contacts. These contact geometries are interesting for different applications. Si–Si contacts are essential for all electrically connected devices, where well-defined thermal, electrical, and mechanical properties are required from the contacts. The nanogap architecture can be used for field emission sensors. The small droplet that can persist within the nanogap can be used to grow a nanowire within the gap that is narrower than the original nanowire, creating interesting possibilities for hierarchical structures. Such an approach can be useful for developing field effect devices like gas sensors. Si–Au–Si contacts enable the formation of Ohmic contacts and are useful in diffusion studies.

We find that electromigration is the most reliable method for creating controlled contact geometries. A benefit of using electromigration is that direct observation, as in the TEM experiments here, is not essential to create controlled contact geometries. When a nanowire impinges on the contact site, a current driven through the nanowire by a small applied voltage could be used to indicate the progress of contact formation. A timed current pulse can then reduce the AuSi volume to control the contact diameter. Similarly, nanogap formation can be detected without direct observation by monitoring the interruption of current through the nanowire.

A key difference between VLS growth of nanowires in a conventional CVD reactor and the in situ UHV-TEM growth used here is the pressure difference, which can be  $\sim 4$  orders of magnitude. The higher Si growth rates due to higher pressure and the absence of thermo- and electromigration of Au in conventional CVD reactors is more likely to create bulged or straight contacts.<sup>13,14</sup> Furthermore, under the TEM conditions the Au sidewall coating likely has a strong influence on the nanowire electrical properties. This is less of an issue at high silane pressures in a CVD reactor where the SiNWs do not have Au decorated sidewalls.<sup>31,32</sup>

The Si cantilever heaters with localized hot regions used here are an interesting option for post processing integration of individual VLS nanowires into temperature-sensitive CMOS devices and lab-on-a-chip with polymer fluid channels. The high temperatures required for nanowire growth are localized so that the main device remains within its temperature limits (450 °C for CMOS and 100–150 °C for many polymers). The pristine, oxide-free nanowires that are electrically connected at their two ends in the UHV-TEM also make an interesting platform for surface functionalization studies that, for example, can benefit the fields of biosensors and nanowire based solar cells.

## ■ ASSOCIATED CONTENT

### 📄 Supporting Information

The Supporting Information is available free of charge on the ACS Publications website at DOI: 10.1021/acs.nanolett.5b02178.

Information on the design, fabrication, operation, and calibration of cantilever heaters, additional details of the method used to grow Si nanowires in situ, discussion on Au migration mechanism, and further experimental evidence of dominance of electromigration over other processes. (PDF)

Movie 1: The contact formation process for a straight contact. (AVI)

Movie 2: The contact formation process for a necked contact. (AVI)

## ■ AUTHOR INFORMATION

### Corresponding Authors

\*E-mail: [Kristian.Molhave@nanotech.dtu.dk](mailto:Kristian.Molhave@nanotech.dtu.dk) (K.M.).

\*E-mail: [fmross@us.ibm.com](mailto:fmross@us.ibm.com) (F.M.R.).

### Notes

The authors declare no competing financial interest.

## ■ ACKNOWLEDGMENTS

This work was part of the FTP Nano Live project, which was funded by The Danish Council for Independent Research (Case No.10-083797). This work was (partly) supported by The Danish National Research Foundation's Center for Individual Nanoparticle Functionality, CINP (DNRF54).

## ■ REFERENCES

- (1) Wagner, R. S.; Ellis, W. C. *Appl. Phys. Lett.* **1964**, *4* (5), 89.
- (2) Cui, Y.; Zhong, Z.; Wang, D.; Wang, W. U.; Lieber, C. M. *Nano Lett.* **2003**, *3* (2), 149–152.
- (3) Tian, B.; Zheng, X.; Kempa, T. J.; Fang, Y.; Yu, N.; Yu, G.; Huang, J.; Lieber, C. M. *Nature* **2007**, *449* (7164), 885–889.
- (4) Chan, C. K.; Peng, H.; Liu, G.; McIlwrath, K.; Zhang, X. F.; Huggins, R. A.; Cui, Y. *Nat. Nanotechnol.* **2008**, *3* (1), 31–35.
- (5) Svensson, C. P. T.; Mårtensson, T.; Trägårdh, J.; Larsson, C.; Rask, M.; Hessman, D.; Samuelson, L.; Ohlsson, J. *Nanotechnology* **2008**, *19* (30), 305201.
- (6) Duan, X.; Huang, Y.; Agarwal, R.; Lieber, C. M. *Nature* **2003**, *421* (6920), 241–245.
- (7) Hayden, O.; Agarwal, R.; Lieber, C. M. *Nat. Mater.* **2006**, *5* (5), 352–356.
- (8) Dávila, D.; Tarancón, A.; Fernández-Regúlez, M.; Calaza, C.; Salleras, M.; Paulo, A. S.; Fonseca, L. J. *Micromech. Microeng.* **2011**, *21* (10), 104007.
- (9) Li, M.; Bhiladvala, R. B.; Morrow, T. J.; Sioss, J. A.; Lew, K.-K.; Redwing, J. M.; Keating, C. D.; Mayer, T. S. *Nat. Nanotechnol.* **2008**, *3* (2), 88–92.
- (10) Wang, Z. L.; Song, J. *Science* **2006**, *312* (5771), 242–246.
- (11) Zheng, G.; Patolsky, F.; Cui, Y.; Wang, W. U.; Lieber, C. M. *Nat. Biotechnol.* **2005**, *23* (10), 1294–1301.
- (12) Skucha, K.; Fan, Z.; Jeon, K.; Javey, A.; Boser, B. *Sens. Actuators, B* **2010**, *145* (1), 232–238.
- (13) Chaudhry, A.; Ramamurthi, V.; Fong, E.; Islam, M. S. *Nano Lett.* **2007**, *7* (6), 1536–1541.
- (14) Sharma, S.; Kamins, T. I.; Islam, M. S.; Williams, R. S.; Marshall, A. F. *J. Cryst. Growth* **2005**, *280* (3–4), 562–568.
- (15) Kallesøe, C.; Wen, C.-Y.; Booth, T. J.; Hansen, O.; Bøggild, P.; Ross, F. M.; Mølhave, K. *Nano Lett.* **2012**, *12* (6), 2965–2970.
- (16) Quitoriano, N. J.; Kamins, T. I. *Nano Lett.* **2008**, *8* (12), 4410–4414.
- (17) Fernandez-Regulez, M.; Sansa, M.; Serra-Garcia, M.; Gil-Santos, E.; Tamayo, J.; Perez-Murano, F.; Paulo, A. S. *Nanotechnology* **2013**, *24* (9), 095303.
- (18) Feng, X. L.; He, R.; Yang, P.; Roukes, M. L. *Nano Lett.* **2007**, *7* (7), 1953–1959.
- (19) Kamins, T. I.; Sharma, S.; Yasseri, A. A.; Li, Z.; Straznicki, J. *Nanotechnology* **2006**, *17* (11), S291.

- (20) Kallesøe, C.; Wen, C.-Y.; Mølhave, K.; Bøggild, P.; Ross, F. M. *Small* **2010**, *6* (18), 2058–2064.
- (21) Mølhave, K.; Wacaser, B. A.; Petersen, D. H.; Wagner, J. B.; Samuelson, L.; Bøggild, P. *Small* **2008**, *4* (10), 1741–1746.
- (22) Edgar, C. W.; Islam, M. S. *Proc. SPIE* **2005**, *6003*, 60030P–60030P-11.
- (23) Erdem Alaca, B. *Int. Mater. Rev.* **2009**, *54* (5), 245–282.
- (24) Ross, F. M. *Rep. Prog. Phys.* **2010**, *73* (11), 114501.
- (25) Schmidt, V.; Wittemann, J. V.; Gösele, U. *Chem. Rev.* **2010**, *110* (1), 361–388.
- (26) Kodambaka, S.; Tersoff, J.; Reuter, M. C.; Ross, F. M. *Phys. Rev. Lett.* **2006**, *96*, 096105 .
- (27) Okamoto, H.; Massalski, T. B. *Bull. Alloy Phase Diagrams* **1983**, *4* (2), 190–198.
- (28) Kim, B. J.; Tersoff, J.; Kodambaka, S.; Jang, J.-S.; Stach, E. A.; Ross, F. M. *Nano Lett.* **2014**, *14* (8), 4554–4559.
- (29) Kimukin, I.; Islam, M. S.; Williams, R. S. *Nanotechnology* **2006**, *17* (11), S240–S245.
- (30) Wiethoff, C.; Ross, F. M.; Copel, M.; Horn-von Hoegen, M.; Meyer zu Heringdorf, F.-J. *Nano Lett.* **2008**, *8* (9), 3065–3068.
- (31) Den Hertog, M. I.; Rouviere, J.-L.; Dhalluin, F.; Desré, P. J.; Gentile, P.; Ferret, P.; Oehler, F.; Baron, T. *Nano Lett.* **2008**, *8* (5), 1544–1550.
- (32) Madras, P.; Dailey, E.; Drucker, J. *Nano Lett.* **2010**, *10* (5), 1759–1763.